

*Paleoceanography*

Supporting Information for

New Constraints on Deglacial Marine Radiocarbon Variability from a Depth  
Transect near Baja California

Colin M. Lindsay (Colin.Lindsay@colorado.edu)<sup>1,2</sup>, Scott J. Lehman<sup>2</sup>, Thomas M.  
Marchitto<sup>1,2</sup>, José D. Carriquiry<sup>3</sup>, Joseph D. Ortiz<sup>4</sup>

<sup>1</sup>Department of Geological Sciences, University of Colorado, Boulder, CO 80309,  
USA.

<sup>2</sup>Institute of Arctic and Alpine Research, University of Colorado, Boulder, CO  
80309, USA.

<sup>3</sup>Instituto de Investigaciones Oceanológicas, Universidad Autónoma de Baja  
California, Ensenada, Mexico

<sup>4</sup>Department of Geology, Kent State University, Kent, OH 44242, USA.

**Contents of this file**

Text S1 to S3  
Figures S1 to S3

**Additional Supporting Information (Files uploaded separately)**

Caption for Dataset S1

**Introduction**

The supporting information here provides details on the method by which the suite of cores from near Baja California were placed on a common age model. It also provides more details on the new  $\delta^{13}\text{C}$  record from core PC08 and describes how the  $\delta^{18}\text{O}$  records from near Baja California and the Galapagos Rise were adjusted for small differences in density between their core locations and the Santa Barbara Basin prior to being used to calculate the estimate of deglacial Equatorial Pacific  $\Delta^{14}\text{C}$  described as “Scenario 3” in the main text.

## **Text S1.**

### Age Modeling Supplementary Methods

As described in section 2.4, calendar age models for cores PC10 and GC38 were constructed primarily by mapping  $^{14}\text{C}$  *G. ruber* measurements onto the *G. ruber*  $^{14}\text{C}$  record of PC08, supplemented where necessary by tie points based on the sediment reflectance (Figures S1 and S2). The PC08 *G. ruber* reference curve (light-blue shaded fields in Figures S1 and S2) was constructed by interpolating the PC08 *G. ruber*  $^{14}\text{C}$  age vs. the previously-published GISP2-tied calendar age model [Marchitto *et al.*, 2007] using a Monte-Carlo approach. Similar to our method of interpolating age models (see section 2.4), the low-frequency variability in the rate of change ( $^{14}\text{C}$  years / calendar year) within PC08 was used as an approximation of the high-frequency variability, which when input to the Monte Carlo algorithm allowed us to estimate the larger uncertainty of the reference curve between control points. Because there is no planktic material available in the early Holocene section of PC08, three benthic measurements were included in the interpolation. This effectively assigned a minimum age to the youngest *G. ruber* dates that mapped onto the youngest part of the reference curve, ensuring that the age models for PC10 and GC38 would not result in *G. ruber* surface  $\Delta^{14}\text{C}$  values implausibly lower than coeval PC08 (705m water depth) benthic  $\Delta^{14}\text{C}$ .

## **Text S2.**

### PC08 benthic $\delta^{13}\text{C}$

The  $\delta^{13}\text{C}$  of intermediate waters was at a minimum during the last deglaciation in the eastern equatorial Pacific (Carriviry *et al.*, 2015; Mix *et al.* 1991). The  $\delta^{13}\text{C}$  of *Uvigerina perigrina* from core MV99/GC31/PC08 reaches its lowest values between 20 and 10ka, but the deglacial minimum is punctuated by heavier values during Heinrich Stadial 1 (HS1) and the Younger Dryas (YD; see Figure S3, left axis). This is likely due to changes in porewater concentrations of respired (low- $\delta^{13}\text{C}$ ) carbon varying the isotopic offset between porewaters and

bottom water in response to changes in local export productivity. In Figure S3 we compare  $\delta^{13}\text{C}$  from cores PC08 and GC31 to Factor 3 of the diffuse spectral reflectance (DSR), which is correlated with organic carbon content of the core sediments and local export productivity [Ortiz *et al.*, 2004] The comparison suggests that lower productivity, and thus a smaller porewater offset, during HS1 and the YD may have caused the infaunal *U. perigrina* to record heavier  $\delta^{13}\text{C}$  during those periods, overprinting the regional deglacial  $\delta^{13}\text{C}$  minimum.

### **Text S3.**

The Modern Gradient  $\delta^{18}\text{O}$  of Calcite between SBB and Galapagos Rise  
In the modern ocean, the  $\delta^{18}\text{O}$  of seawater in the tropical Pacific regresses onto salinity with a slope of 0.27 ‰/psu [LeGrande and Schmidt, 2006]. Multiplying by the salinity difference between SBB and Galapagos Rise core VM21-30 core locations (~0.3 psu, Fig. 2 in the main text) suggests that SBB seawater  $\delta^{18}\text{O}$  should be ~0.1 ‰ lower than at Galapagos Rise. The temperature effect on the  $\delta^{18}\text{O}$  of calcite would oppose the seawater  $\delta^{18}\text{O}$  gradient, because intermediate water at the equator is generally warmer than at SBB. Multiplying the temperature difference between SBB and Galapagos Rise core locations (1.2°C, Fig. 2 in the main text) by a typical temperature calibration of 0.25 ‰/°C [Bemis *et al.*, 1998] adds 0.3 ‰, with the result that modern Galapagos Rise  $\delta^{18}\text{O}$  of calcite should be ~0.2‰ lighter than at SBB, a small offset relative to the scatter in downcore  $\delta^{18}\text{O}$  data (Fig. 7 in the main text). Galapagos Rise core VM21-30 and Baja California core PC08 are at slightly deeper, colder density levels than the SBB sill depth (Fig. 3 in the main text), by approximately 0.6 and 1 °C respectively. Using the same temperature calibration, we therefore subtracted 0.15 and 0.25‰ from the VM21-30 and PC08  $\delta^{18}\text{O}$  splines before calculating the mixing ratios for Scenario 3 described in section 3.6 in the main text.

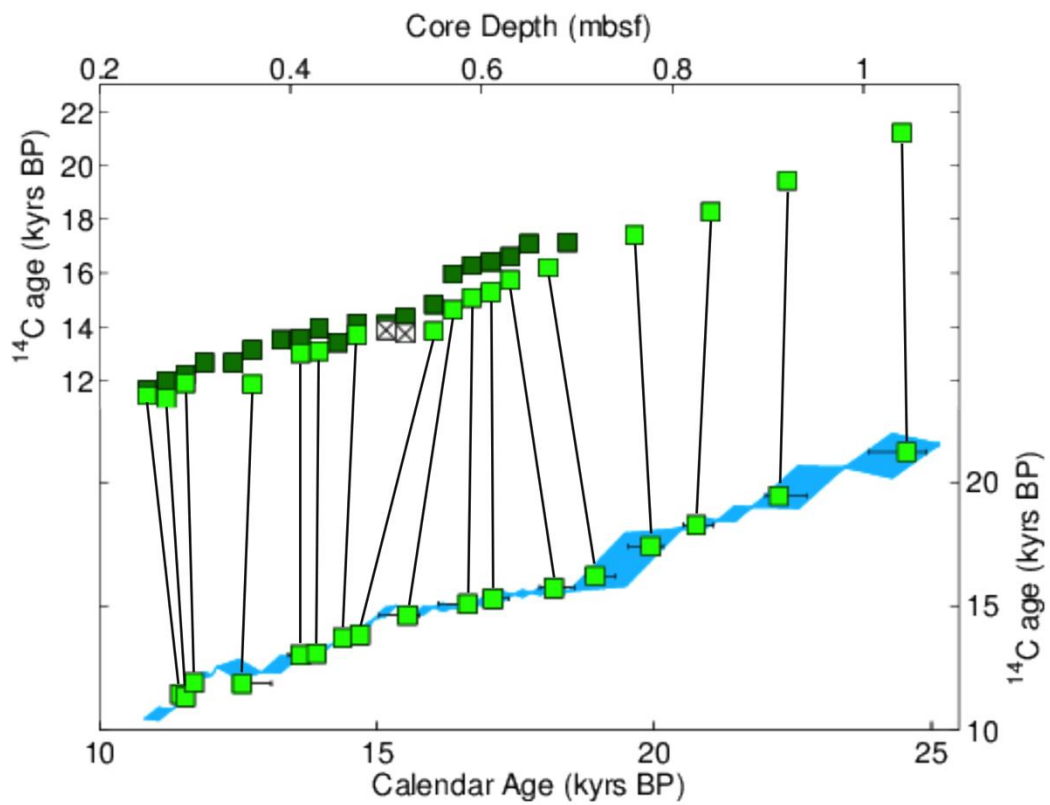
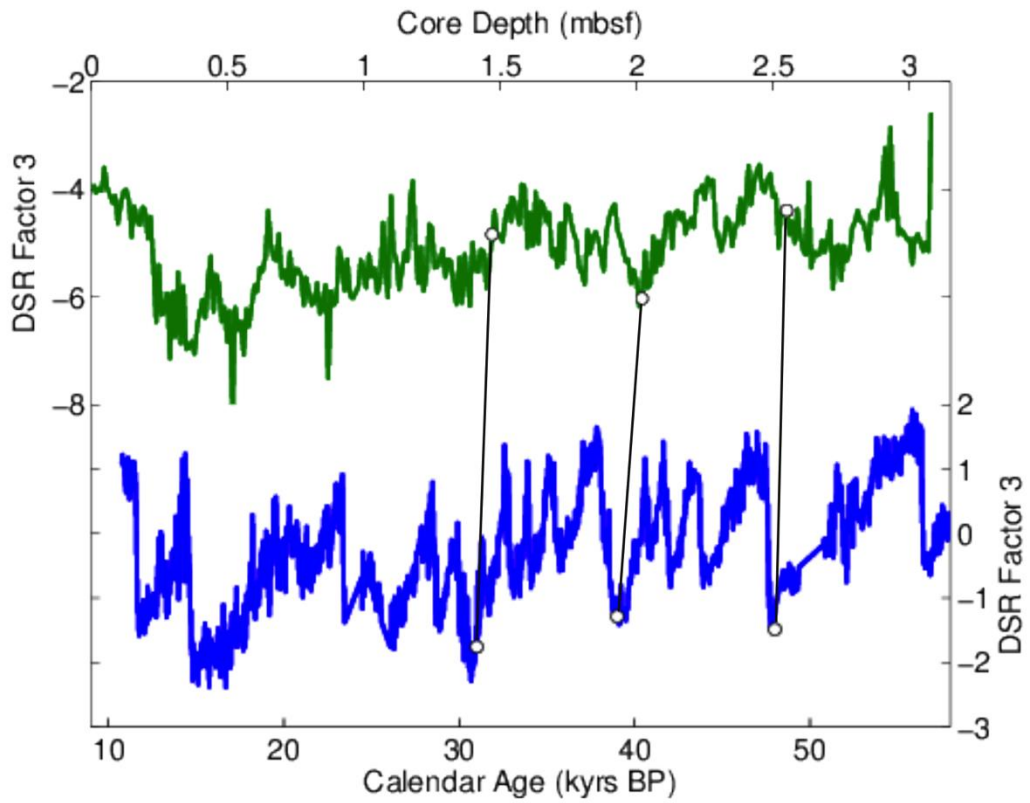


**Figure S1.** Top axes: DSR Factor 3 tiepoints used to place GC38 (green, vs. depth in core on top axis) onto the age model of core PC08 (blue, vs. calendar age on the bottom axis). Bottom axes: Deglacial GC38 *Uvigerina* (dark green squares) and *G. ruber* (light green squares and white squares with Xs)  $^{14}\text{C}$  measurements vs. depth in core (top axes). Tiepoints to the PC08 *G. ruber  $^{14}\text{C}$  reference curve (light blue shape vs. calendar age on the lower axis) represent the results of our Monte Carlo age modeling. The *G. ruber  $^{14}\text{C}$  measurements that were used in the age model are plotted again (light green squares on the lower axis) with the resulting horizontal calendar age error bars. The white**

squares with Xs are *G. ruber* measurements not used in the age modeling. Note that the scales of the top and bottom x-axes are different.

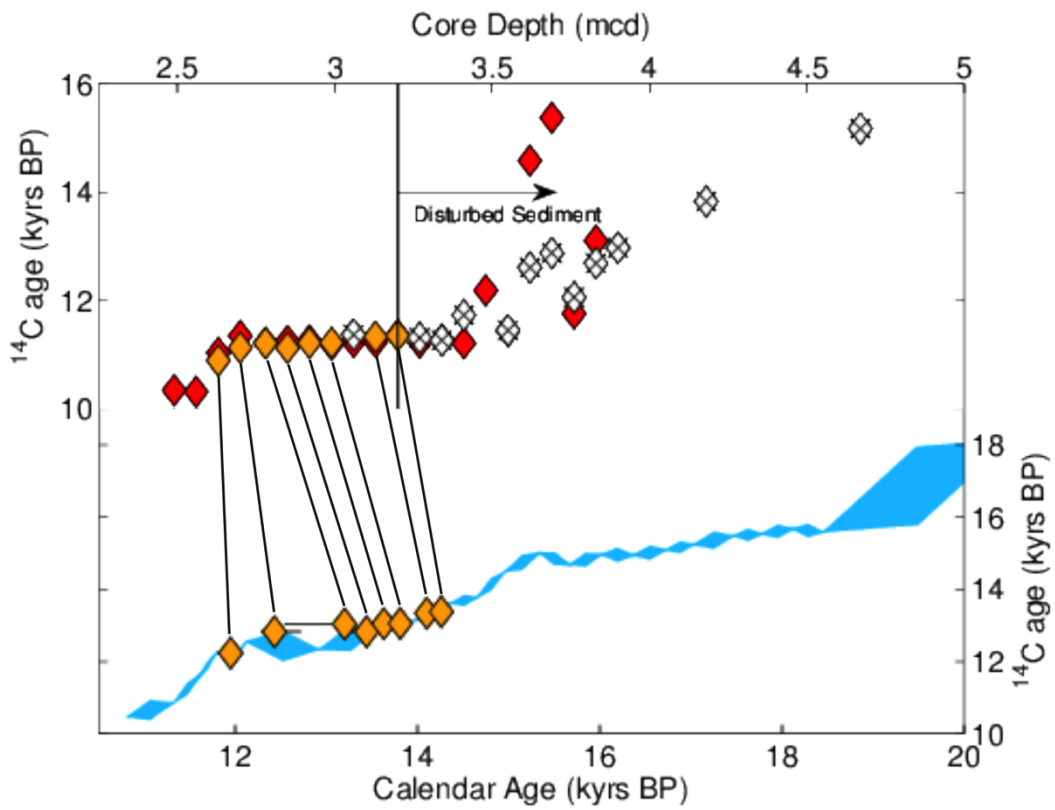
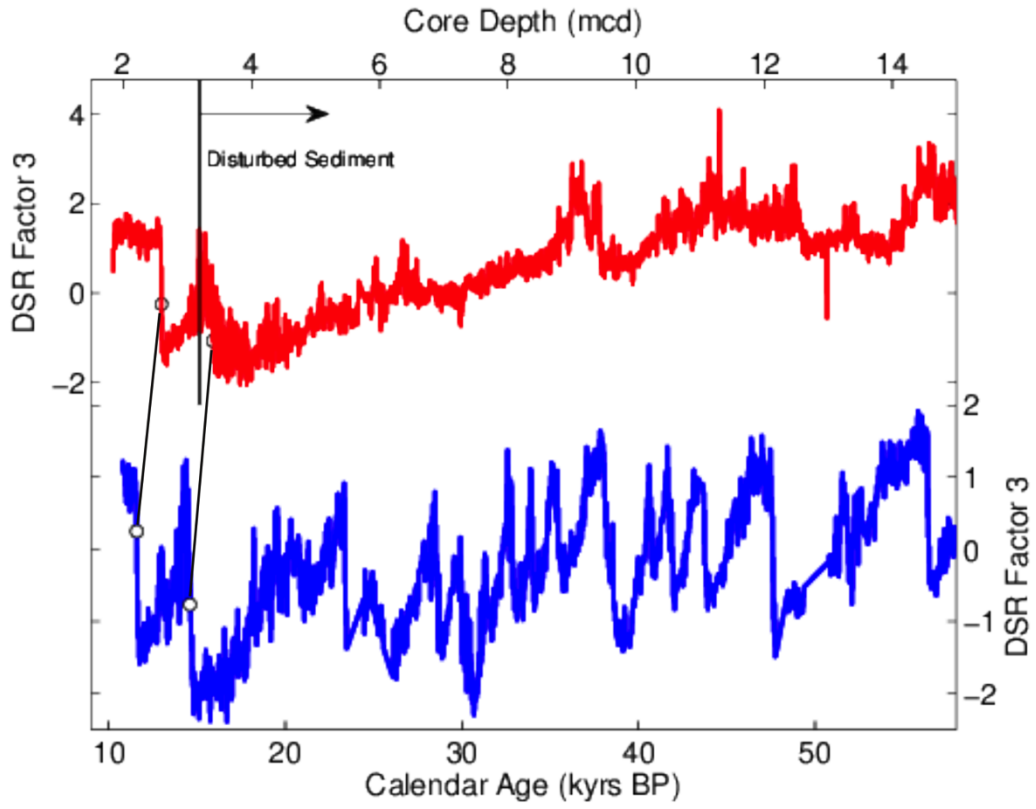


**Figure S2.** Top axes: DSR Factor 3 tiepoints used to place PC10 (red, vs. composite depth on top axis) onto the age model of core PC08 (blue, vs. calendar age on the bottom axis). Bottom axes: PC10 *Uvigerina* (red diamonds) and *G. ruber* (orange diamonds and white diamonds with Xs)  $^{14}\text{C}$  measurements vs. composite depth (top axes). Tiepoints to the PC08 *G. ruber*  $^{14}\text{C}$  reference curve (light blue shape vs. calendar age on the lower axis) represent the results of our Monte Carlo age modeling. The *G. ruber*  $^{14}\text{C}$  measurements that were used in the age model are plotted again (orange diamonds on the lower axis) with the resulting horizontal calendar age error bars. The white diamonds with overlaid X markers are *G. ruber* measurements not used in the age modeling. Note that the scales of the top and bottom x-axes are different.

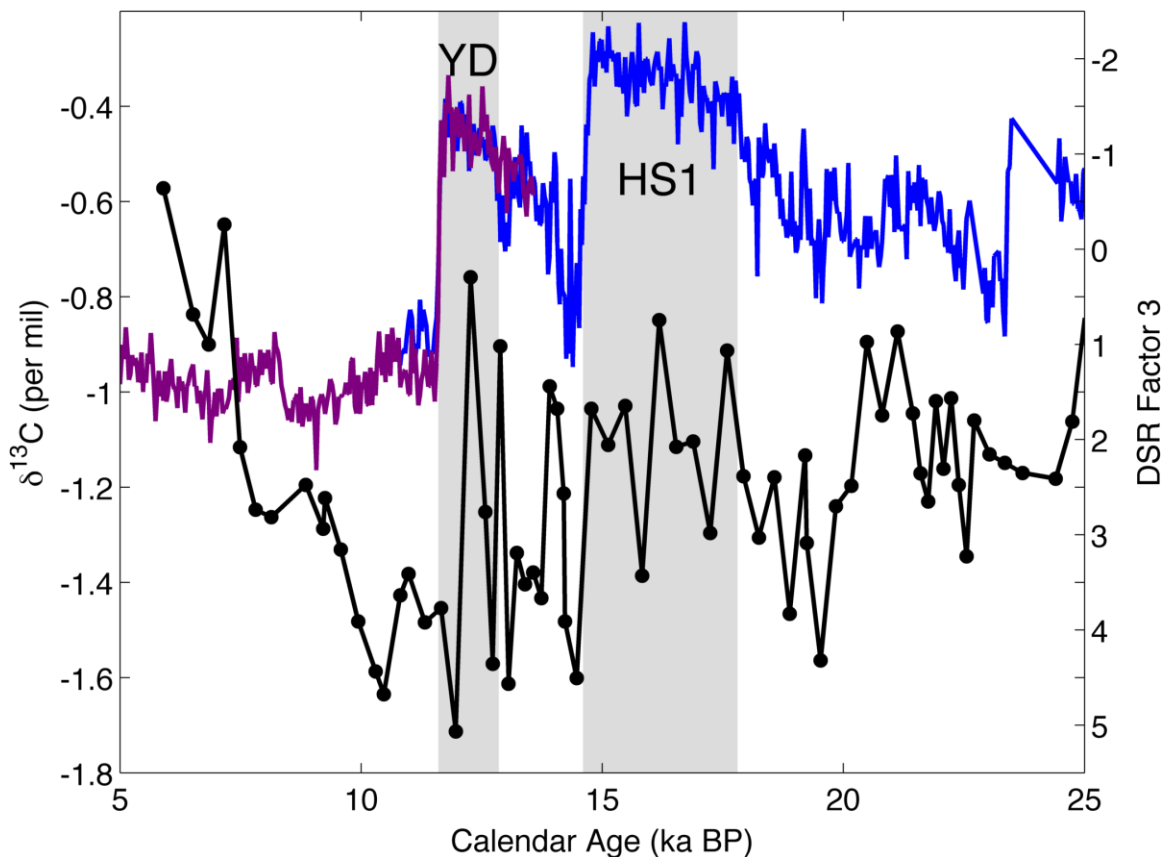


**Figure S3.** PC08 and GC31 DSR Factor 3 (blue and purple lines, right reversed axis) compared to PC08 and GC31  $\delta^{13}\text{C}$  measured in *Uvigerina* spp. Gray fields indicate Heirich Stadial 1 (HS1) and the Younger Dryas (YD). High DSR values are associated with higher organic carbon content in the cores and were likely caused by greater local export productivity.

**Data Set S1.** Excel file containing the  $^{14}\text{C}$  measurements from Baja California cores MV99-PC10 and MV99-GC38 that are presented in this paper, as well as the  $\delta^{18}\text{O}$  record from composite core MV99-MC19/GC31/PC08 and DSR tie-points used to place the cores on a common calendar age model.